*Journal of Groundwater Science and Engineering* 12(2024) 190–204

Journal homepage: http://gwse.iheg.org.cn

# Characteristics and genesis of groundwater salinization in coastal areas of the Lower Reaches of Oujiang Basin

Mei-hui Zhang[1,2,3], Shi-yang Zhou[4], Dan-dan Liu[5*], Ying Zhang[1,2], Yu-xi Zhang[1,2], Xi Chen[1,2], Hui-wei Wang[1,2], Bei Li[1,2], Wei Kang[1,2], Bing Yi[1,2,3], Wan-peng Shi[6]

[1] *Institute of Hydrogeology and Environmental Geology*, *Chinese Academy of Geological Sciences*, *Shijiazhuang* 050061, *China*..
[2] *Fujian Provincial Key Laboratory of Water Cycling and Eco–Geological Processes*, *Xiamen* 361021, *Fujian* , *China*.
[3] *China University of Geosciences (Beijing)*, *Beijing* 100083, *China*.
[4] *Changsha Center of Natural Resources Comprehensive Survey*, *China Geological Survey*, *Changsha* 410600, *China*.
[5] *Hydrogeological Environmental Geological Survey Center of China Geological Survey*, *Tianjin* 071501, *China*.
[6] *China University of Geosciences*, *Wuhan* 430074, *China*.

**Abstract:** The coastal areas of the lower reaches of Oujiang River Basin are rich in groundwater resources. However, the unsustainable exploitation and utilization of groundwater have led to significant changes in the groundwater environment. Understanding the characteristics and genesis of groundwater salinization is crucial for preventing its deterioration and ensuring sustainable utilization. In this study, a comprehensive approach combining the ion ratio method, mineral saturation index method and multivariate statistical analysis was employed to investigate the hydrochemical characteristics and main controlling factors in the study area. The findings reveal that: (1) Groundwater samples in study area exhibit a neutral to slightly alkaline pH. The predominant chemical types of unconfined water are $HCO_3$-Ca·Na, $HCO_3$·Cl-Na·Ca and $HCO_3$·$SO_4$-Ca·Na, while confined water mainly exhibits Cl·$HCO_3$-Na and Cl-Na types. (2) Salinity coefficients indicate an increase in salinity from unconfined to confined water. TDS, $Na^+$ and $Cl^-$ concentrations show an increasing trend from mountainous to coastal areas in unconfined water, while confined water displays variability in TDS, $Na^+$ and $Cl^-$ concentrations. (3) Groundwater salinity is mainly influenced by water-rock interactions, including the dissolution of halite and gypsum, cation exchange, and seawater intrusion etc. Additionally, human activities and carbonate dissolution contribute to salinity in unconfined water. Seawater intrusion is identified as the primary factor leading to higher salinity in confined water compared to unconfined water, with increasing cation exchange and seawater interaction observed from unconfined to confined water.

**Keywords:** Hydrochemical; Multivariate statistical analysis; Seawater intrusion

Received: 19 Oct 2023/ Accepted: 26 Apr 2024/ Published: 10 Jun 2024

## Introduction

Groundwater serves as a critical resource for sustaining human activities, economic development, and maintaining the stability of coastal ecosystem and water resource security (Wang, 2019; Alhassan et al. 2018). However, due to the impacts of global climate change, sea level rise, and human activities, groundwater related environmental issues in coastal areas have escalated, with groundwater salinization emerging as a significant ecological and geological concern worldwide (Trabelsi and Zouari, 2019; Bahir and Ouhamdouc, 2020; Thilagavathi et al. 2021). Elevated salt levels in groundwater not only impede industrial development and escalate operational expenses but also lead to land salinization and adversely affect agricultural production. Furthermore, contamination of drinking water sources by highly saline groundwater poses health risks, potentially straining kidneys and increasing the risk of liver damage (Jabed et al. 2018; Troudi et al. 2020). The salinization of groundwater originates from various factors, including transgression-regressive events related to paleo-seawater intrusion (Larsen et al. 2017), modern seawater intrusion (Dang, 2022); pollution

*Corresponding author: Dan-dan Liu, *E-mail address*: liudandan@mail.cgs.gov

DOI: 10.26599/JGSE.2024.9280015

Zhang MH, Zhou SY, Liu DD, et al. 2024. Characteristics and genesis of groundwater salinization in coastal areas of the Lower Reaches of Oujiang Basin. Journal of Groundwater Science and Engineering, 12(2): 190-204.

from industrial and domestic wastewater (Zamrsky et al. 2020); evaporation and concentration (Ez-Zaouy et al. 2022) and water-rock interactions (Sun et al. 2023).

Hydrochemical analysis methods provide valuable insights into the causes of groundwater salinization. Zhang et al. (2013) conducted a study in the Yangday River plain area of Qinhuangdao, analyzing the chemical characteristics of groundwater and seawater using mathematical statistics. They identified electrical conductivity, chloride ions, dissolved total solids and potential salinity as the most reliable indicators for assessing seawater intrusion. Additionally, they established corresponding background values and a ranking system. Kazakis (2016) employed hydrogeochemical and geophysical methods to investigate the extent and characteristics of seawater intrusion in the aquifer along the eastern coast of Thermaikos Bay, Greece, and found that the depth of seawater intrusion can reach 200 m. Zhang et al. (2017) used hydrochemical analysis and isotope methods to delve into the multiple influencing factors of deep groundwater salinization in Yancheng area, and their results highlighted significant regional variations in the degree of groundwater salinization, indicating diverse underlying causes.

After extensive research into the environmental geological issues of the Oujiang River Basin in Zhejiang Province, scholars have identified serious irrational exploitation and utilization of groundwater in the downstream cities of the basin. While the distribution and proportion of underground saline water have been studied, the precise cause of salinity remain unclear. The Oujiang Estuary area experienced the largest seawater intrusion event in its history during the Holocene, further aggravating the issue of groundwater salinization (Zhu, 2009). Despite previous studies on groundwater development and utilization (Jia et al. 2007), as well as surface and groundwater water quality (Pan, 2020; Li et al. 2023) in this area, there remains a lack of research on geochemical changes and causes of groundwater salinity characteristics. To address this gap, this paper employs traditional hydrochemical analysis and multivariate statistical analysis to comprehensively investigate ion ratios, mineral saturation indices and other factors. The aim is to further investigate the saline characteristics, material sources and controlling factors of groundwater at different depths, providing theoretical guidance for the rational development, utilization and protection of groundwater resources in the lower reaches of the Oujiang River basin.

## 1 Study area

The study area is located in the lower reaches of Oujiang River Basin of Wenzhou City in the southeast of Zhejiang Province, China. Spanning between longitudes 119°08' E and 121°12' E and latitudes 27°04' N and 28°38' N, the investigated region encompasses diverse geographical features. The lower reaches of Oujiang River Basin are characterized by middle to low mountain and hilly terrain. The landscape slopes gently from southwest to northeast, forming a trapezoidal shape. The plain areas are relatively low-lying and flat, with a slight incline from the mountain fronts towards the sea. The study area experiences a subtropical oceanic monsoon climate, with a mean annual precipitation of approximately 1,800 mm.

Under the influence of natural factors such as topography, geological formation, and lithology, groundwater in the study area is predominantly categorized into three types: Porous aquifers in loose rock, porous-fissure aquifers of clastic rock and fissure aquifers in bedrock (Fig. 1). Groundwater in the study area primarily originates from porous aquifers in loose rock. The Wenzhou area is situated within the South China stratum, characterized by abundant pyroclastic rocks. The Upper Jurassic Moshan Group comprises sandy conglomerate and siltstone. Calcareous sedimentary rocks of the Lower Cretaceous Yongkang Group contain andesite, sandstone and gravel. The locally dispersed metamorphic complexes of the Upper Paleozoic consist mainly of Muscovite schist and Muscovite quartz schist. The Quaternary strata in the study area comprise pebbles, gravel, sand and soil layers, with thickness ranging from tens of meters to 170 m. Groundwater in the study area transitions from unconfined water in the piedmont plain to unconfined and confined aquifers in the coastal plain (Fig. 2). The fore-mountain aquifer is predominated composed of alluvial sand and gravel, while the plain aquifer consists mainly of alluvial deposit and marine clay soil rich in iron and manganese, partially composed of fine sand. Confined water is primarily distributed in the southern part of the study area, with lithology mainly comprising alluvial gravel from the late Pleistocene aquifer.

In the valley and plain area in front of mountains, the unconfined water mainly receives vertical recharge from atmospheric precipitation, irrigation water, surface water and fissure aquifers in bedrock. Discharge of unconfined water in these areas mainly occurs through artificial exploitation and drainage to surface water bodies. In the coastal

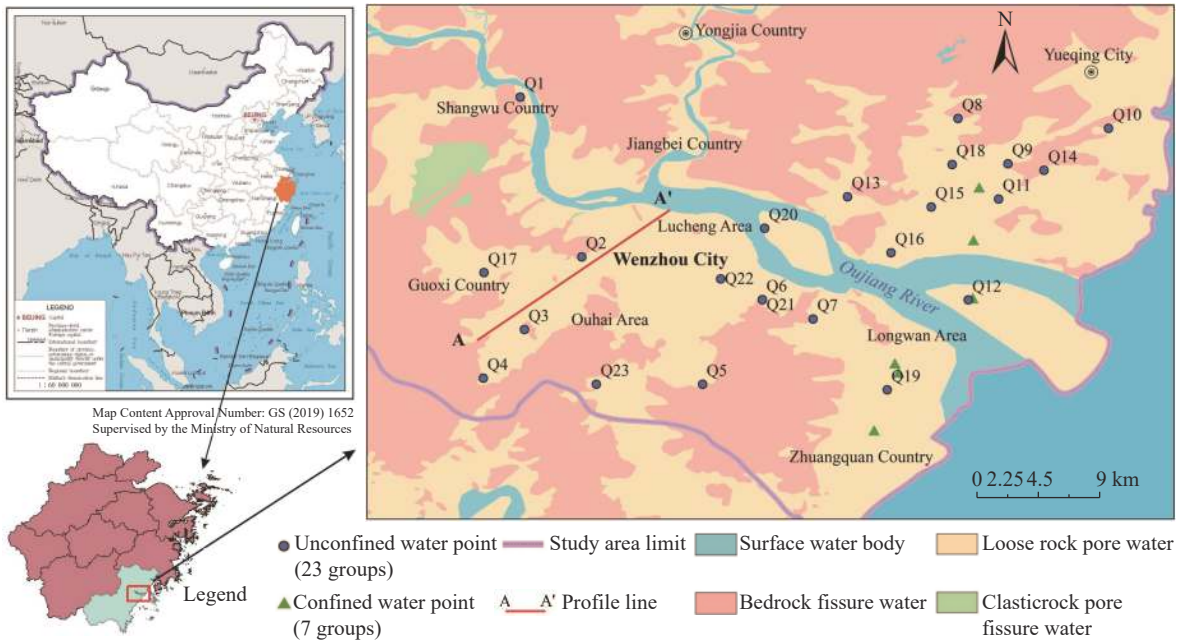


**Fig. 1** Schematic map of hydrogeology and locations of sampling points in the study area

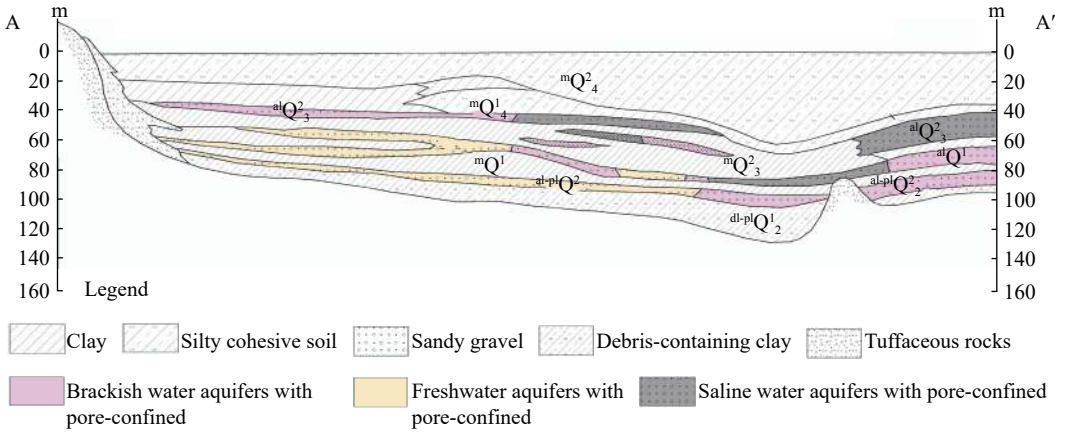


**Fig. 2** The hydrogeological cross section along the A-A′ in the study area

plain, unconfined water is primarily recharged by atmospheric precipitation and surface water. However, runoff conditions in the coastal plain are relatively poor, and the discharge methods mainly involve water extraction from private wells and evapotranspiration. The confined water aquifer is covered by a thick layer of impermeable soil, limiting vertical infiltration and recharge from atmospheric precipitation, surface water and shallow pore water. Moreover, confined water is distant from the upstream recharge area, and the hydraulic gradient is extremely gentle, resulting in weak lateral recharge.

## 2 Materials and methods

### 2.1 Sampling and analysis

In July 2022, this study collected 30 sets of groundwater samples. Among them, 23 unconfined water and 7 confined water samples were collected from the study area. All unconfined water samples were collected from wells with depths of 1.7 m to 10.9 m, and all confined water samples were collected from drills with depths of 93.8 m to 144.4 m.

Samples were analyzed in the Hubei Geological Research Laboratory for cations ($K^+$, $Na^+$, $Ca^{2+}$, $Mg^{2+}$, $Mn^{2+}$, $NH_4^+$), anions ($Cl^-$, $SO_4^{2-}$, $HCO_3^-$, $NO_3^-$, $Br^-$), pH, Total Dissolves Solids (TDS). Among these paraments, $K^+$, $Na^+$, and $Mn^{2+}$ were measured using inductively coupled plasma emission spectrometer (ICAP-7400). $Ca^{2+}$, $Mg^{2+}$ were determined using ethylenediamine disodium tetraacetic acid titration methods. $NH_4^+$ was measured using visible spectrophotometer (7230G). $Cl^-$, $SO_4^{2-}$, and $NO_3^-$ were measured using ion chromatography (930 Compact IC Flex). The

precision of each ion is 0.01 mg·L$^{-1}$. $HCO_3^-$ was analyzed with the titration method. pH was measured using a pH meter (PHS-3C), with a precision of ±0.01. TDS was determined using the gravimetric method.

## 2.2 Statistical analyses

The hydrochemical characteristics were analyzed and studied by Piper trilinear diagram, while the related causes were analyzed and studied by Gibbs diagram. In this study, the PHREEQC software was utilized to calculate mineral Saturation Index (SI) values. The data were analyzed statistically based on principal component analysis by SPSS (26.0) software. The ion ratio diagrams were generated using Origin. The SI, principal component analysis, and ion ratio diagrams were used to analyze the water-rock interaction of related rocks and determine the main source of groundwater composition.

# 3 Results and discussion

## 3.1 Chemical characteristics of groundwater

### 3.1.1 Chemical statistical characteristics of groundwater

Descriptive statistics were performed on the dataset of unconfined and confined water (Table 1). Obvious differences were observed in the chemical characteristics between unconfined and confined water. The unconfined water samples were neutral to slightly alkaline, with pH values ranging from 6.36 to 8.81. The mean Total Dissolved Solids (TDS) was 350 mg·L$^{-1}$, with the TDS of only sampling point Q19 being 2,254 mg·L$^{-1}$, indicating brackish water located in the middle of Longwan Area on the coastal plain. The TDS of other unconfined water sampling points were less than 1,000 mg·L$^{-1}$, classified as fresh water. The average concentrations of cations and anions were ranked in the order $Na^+ > Ca^{2+} > K^+ > Mg^{2+} > Mn^{2+} > NH_4^+$ and $HCO_3^- > Cl^- > SO_4^{2-} > NO_3^- > Br^-$, Respectively. The concentrations of $Na^+$ and $Ca^{2+}$ were high in the cations, accounting for 53.7% and 23.45% of the total cations, respectively. The concentrations of $HCO_3^-$ and $Cl^-$ were high in the cations, accounting for 59.87% and 29.13% of the total anions, respectively. The number of $Na^+$ and $Cl^-$ exceeding the limit of the Class groundwater quality standard accounted for 8.7% of the unconfined water.

The confined water samples were neutral to slightly alkaline, with pH and TDS value ranging from 6.54 to 7.93 and from 450 mg·L$^{-1}$ to 9,700 mg·L$^{-1}$. The mean TDS was 2,628 mg·L$^{-1}$. Within the confined water samples, 28.6% were classified as fresh water, 57.1% as brackish water, and 14.3% as saline water (3,000 mg·L$^{-1}$ < TDS ≤ 10,000 mg·L$^{-1}$). The average concentrations of cations and anions were ranked in the order $Na^+ > Ca^{2+} > Mg^{2+} > K^+ > NH_4^+ > Mn^{2+}$ and $Cl^- > HCO_3^- > NO_3^- > SO_4^{2-} > Br^-$, respectively. $Cl^-$ was the dominant anion in confined water, accounting for 84.76% of the total anions, followed by $HCO_3^-$, accounting for 14.58% of the total anions, which differed from unconfined water. A comparison between uncon-

**Table 1** Statistics on the content of chemical indices of unconfined and confined water in the lower reaches of Oujiang Basin

| Groundwater type | | pH | TDS | $K^+$ | $Na^+$ | $Ca^{2+}$ | $Mg^{2+}$ | $Cl^-$ | $HCO_3^-$ | $SO_4^{2-}$ | $NO_3^-$–N | $Br^-$ |
|---|---|---|---|---|---|---|---|---|---|---|---|---|
| | | | mg·L$^{-1}$ | | | | | | | | | |
| Standard | | 6.5–8.5 | 1,000 | \(1) | 200 | \ | \ | 250 | \ | 250 | 20 | \ |
| Unconfined water | Min | 6.36 | 60 | 1.63 | 5.65 | 5.53 | 1.12 | 3.36 | 24.14 | 5.05 | ND(2) | ND |
| | Max | 8.81 | 2,254 | 122.00 | 607.50 | 94.03 | 100.06 | 950.41 | 889.87 | 65.26 | 7.44 | 1.41 |
| | Mean | 7.05 | 350 | 15.00 | 70.39 | 30.74 | 13.81 | 88.45 | 181.81 | 24.07 | 2.06 | 0.17 |
| | Median | 6.90 | 148 | 5.36 | 17.46 | 21.20 | 4.22 | 17.29 | 85.51 | 20.69 | 1.71 | 0.00 |
| | SD | 0.60 | 457 | 24.54 | 127.59 | 21.57 | 21.33 | 195.26 | 208.52 | 17.62 | 1.93 | 0.34 |
| | CV/% | 8 | 130 | 164 | 181 | 70 | 154 | 221 | 115 | 73 | 94 | 201 |
| Confined water | Min | 6.54 | 450 | 3.14 | 168.80 | 12.18 | 8.44 | 59.01 | 28.95 | 0.10 | ND | 0.20 |
| | Max | 7.93 | 9,700 | 21.73 | 3,066.00 | 302.67 | 282.70 | 6,393.59 | 414.04 | 8.74 | 4.44 | 5.45 |
| | Mean | 7.41 | 2628 | 11.55 | 719.39 | 114.68 | 100.74 | 1,553.26 | 267.20 | 2.18 | 1.75 | 2.07 |
| | Median | 7.46 | 1,102 | 8.18 | 262.40 | 65.23 | 52.2 | 457.95 | 344.55 | 0.37 | 1.35 | 1.24 |
| | SD | 0.49 | 3,022 | 6.92 | 968.04 | 98.35 | 94.48 | 2,074.70 | 142.50 | 2.92 | 1.73 | 2.12 |
| | CV/% | 7 | 115 | 60 | 135 | 86 | 94 | 134 | 53 | 134 | 99 | 103 |

Note: (1) \: There is no equivalent groundwater quality standard in China. (2) ND, not detected

fined water and confined water revealed that except for $Ca^{2+}$, $NO_3^-$ and $SO_4^{2-}$, the coefficient of variation of other chemical indices in unconfined water was higher than that in confined water.

### 3.1.2 Classification of groundwater

The Piper diagram is a valuable tool for illustrating the hydrochemical characteristics and types of hydrochemical components present in groundwater (Gang et al. 2023). The Piper-Trilinear diagram (Fig. 3) depicts the hydrochemical water types for both unconfined and confined water samples. According to the Shukalev classification, the groundwater chemistry in the study area exhibits relatively dispersed characteristics. The main hydrochemical types observed in unconfined water are $HCO_3$-Ca·Na, $HCO_3$·Cl-Na·Ca, $HCO_3$.$SO_4$-Ca·Na, Cl·$HCO_3$-Na and $HCO_3$·$SO_4$·Cl-Na·Ca, accounting for 22%, 13%, 13%, 9% and 9%, respectively. Meanwhile, the primary hydrochemical types identified in confined water are Cl·$HCO_3$-Na, Cl-Na, $HCO_3$·Cl-Na, Cl-Na·Mg, and $HCO_3$-Na, accounting for 29%、29%、14%、14%、14%, respectively.

Significant differences were observed between the chemical types of unconfined and confined water (Fig. 4). Moving from the mountain front to the coastal area, the chemical types of unconfined water showed a trend of $HCO_3$ → $HCO_3$·$SO_4$ → $HCO_3$·Cl → Cl·$HCO_3$. Similarly, the anions of confined water flowing from the coastal distance to the sea exhibited a trend of $HCO_3$ → $HCO_3$· Cl → Cl·$HCO_3$ → Cl. According to the hydrochemical types, the dominant anion in groundwater within the study area gradually transitions from the $HCO_3$ type to the $Cl^-$ type from the mountain front to the coast.

## 3.2 The degree of salinity of groundwater

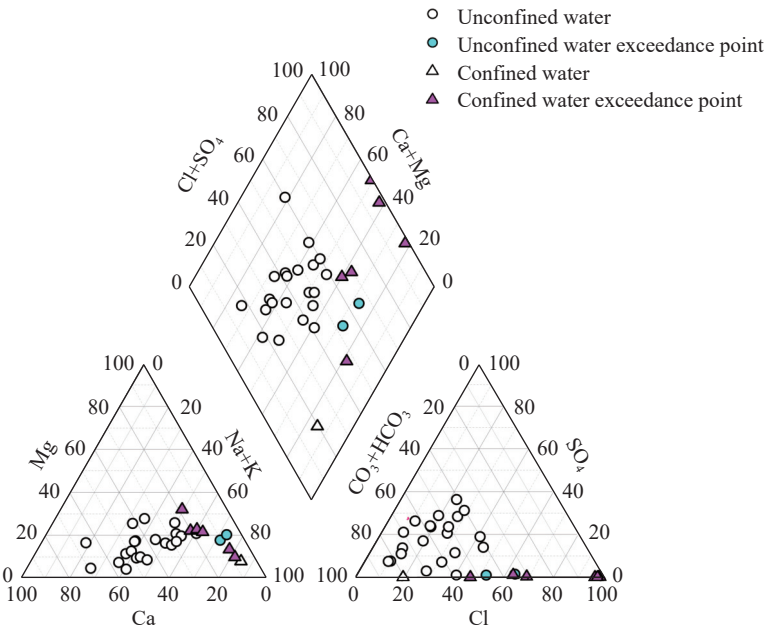


**Fig. 3** Piper diagram of groundwater in the study area

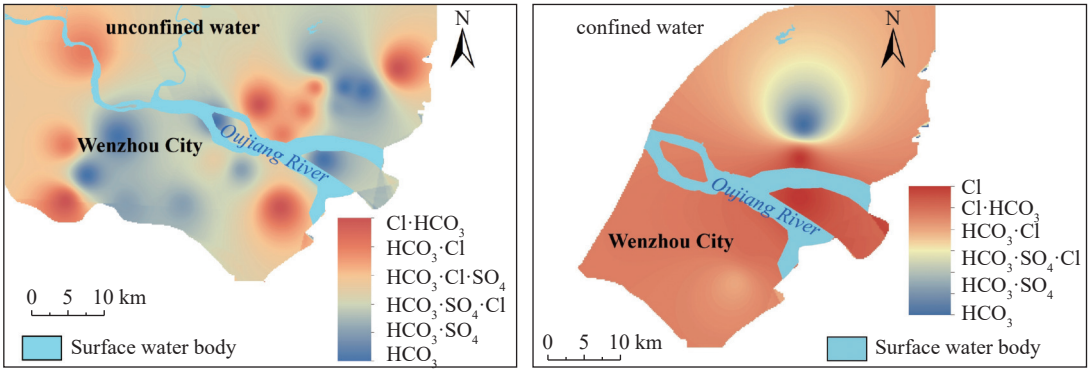


**Fig. 4** Anion hydrochemical type of unconfined and confined water in study area

The Salinization Coefficient (*SC*) was calculated to determine the degree of groundwater salinity. A higher *SC* value indicates a greater degree of groundwater salinity. The formula for calculating *SC* is as follows:

$$SC = \frac{C_{Cl^-}}{C_{HCO_3^-} + C_{CO_3^{2-}}} \quad (1)$$

Where: *SC* is the salinization coefficient of groundwater; $C_{Cl^-}$, $C_{HCO_3^-}$ and $C_{CO_3^{2-}}$ refers to the concentrations of $Cl^-$, $HCO_3^-$ and $CO_3^{2-}$ in groundwater samples, respectively, measured in $mg \cdot L^{-1}$.

The SC range categorizes groundwater into three types: ≤1 for freshwater, 1−2 for brackish water, and >2, for saline water. As shown in Table 2, freshwater predominates in the study area, accounting for 80.00% of the samples. Brackish and saline water are less prevalent, each accounting for 10.00%. Among unconfined water samples, freshwater has the highest proportion (95.65%), followed by brackish water (4.35%), with no samples categorized as saline water. In confined water, the proportion of saline water was the highest (42.86%), followed by freshwater and brackish water (28.57%). Compare to unconfined water, confined water exhibits a higher proportion of saline water.

## 3.3 Spatial distribution characteristics of groundwater salinity

### 3.3.1 Horizontal distribution characteristics of groundwater salinity

The spatial distribution patterns of $Cl^-$, $Na^+$ and TDS in the study area exhibits similarities (Fig. 5). Kriging interpolation analysis conducted in ArcMap10.2 software revealed the spatial distribution characteristics of $Cl^-$, $Na^+$ and TDS in both unconfined and confined water. The results indicate that in unconfined water, higher concentrations of $Cl^-$, $Na^+$ and TDS are observed in the southeast, while lower concentrations are found in the northwest. Moving from the mountains to the coastal plain, the concentrations of $Cl^-$, $Na^+$ and TDS in unconfined water gradually increase, with particularly high concentrations observed in the southern region near the Oujiang River estuary. However, confined water does not exhibit similarly high concentrations of $Cl^-$, $Na^+$ and TDS in the same location. Instead, the distribution of $Cl^-$, $Na^+$ and TDS in confined water shows variations in high and low values (Fig. 5). Generally, compared to unconfined water, confined water tends to have higher concentrations of $Cl^-$, $Na^+$ and TDS, with the high values concentrated in the northern region of the Oujiang River estuary and the surrounding estuary islands.

### 3.3.2 Vertical distribution characteristics of $Cl^-$ in groundwater

The relationship between $Cl^-$ and the depth of water level is analyzed in this study. A dataset comprising 20 sets of unconfined water samples and 7 sets of confined water samples with corresponding groundwater level depth is utilized for this analysis (Fig. 6).

The analysis reveals that the concentration of $Cl^-$ tends to increase with increasing depth, with high $Cl^-$ concentrations predominantly observed in confined aquifers at depth ranging from 100 m to 150 m. In unconfined water, the variation in $Cl^-$ cononcentration ranges from 3.36 $mg \cdot L^{-1}$ to 950.41 $mg \cdot L^{-1}$, with 10.00% of the unconfined water samples exceeding the standard limit. Conversely, in confined water, the variation in $Cl^-$ concentration ranges from 59.01 $mg \cdot L^{-1}$ to 6,393.59 $mg \cdot L^{-1}$, with 71.43% of the confined water samples exceeding the standard limit.

## 3.4 Processes that influence the salinity of groundwater

### 3.4.1 Main controlling factors of groundwater $Cl^-$ enrichment

The chemical composition of groundwater in coastal areas is primarily influenced by precipitation, rock weathering, evaporative concentration, and seawater action (Sheng et al. 2023). The Gibbs diagram is used to analyze the impact of these natural factors by examining the relationship between ions and TDS, thus exploring the ion sources of both unconfined and confined water (Gibbs, 1970).

**Table 2** Salinization coefficient of groundwater

| Salinization | All samples | | Unconfined water | | Confined water | |
|---|---|---|---|---|---|---|
| | Sample number | Ratio/% | Sample number | Ratio/% | Sample number | Ratio/% |
| ≤1 | 24 | 80.00 | 22 | 95.65 | 2 | 28.57 |
| 1~2 | 3 | 10.00 | 1 | 4.35 | 2 | 28.57 |
| >2 | 3 | 10.00 | 0 | 0.00 | 3 | 42.86 |

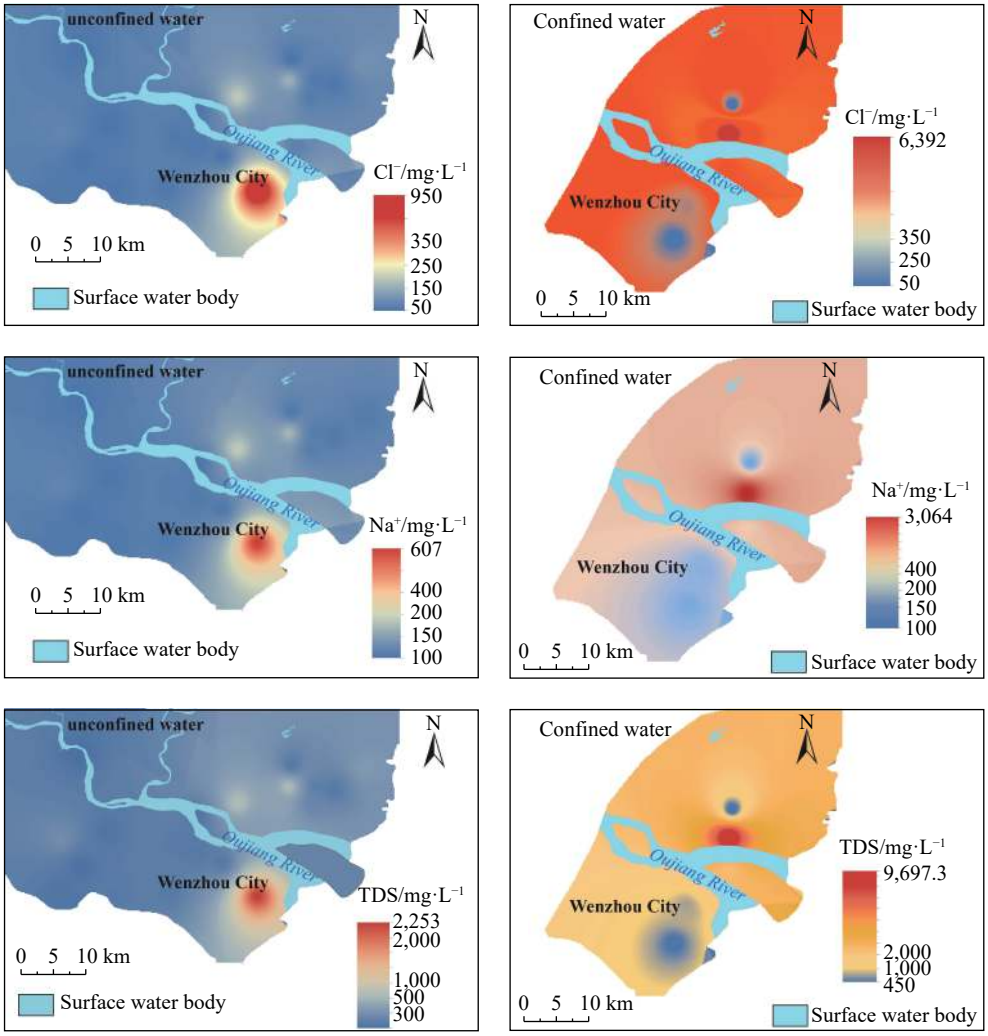


**Fig. 5** Spatial distribution of main ions in unconfined and confined water

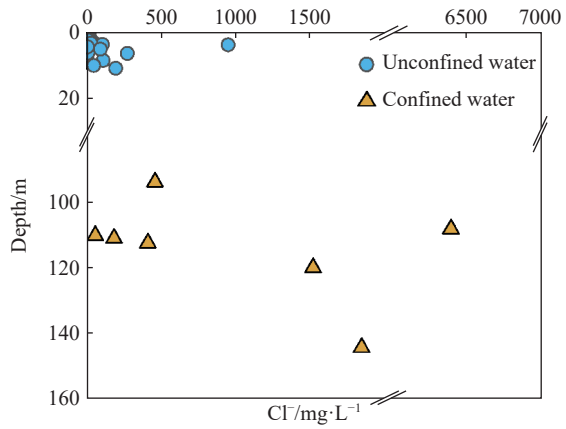


**Fig. 6** The relationship between $Cl^-$ and depth in groundwater

It is observed that in both unconfined and confined water, the ratios of $Na^+/(Na^+{+}Ca^{2+})$ cation mass concentration ranged from 0.19 to 0.92 and 0.74 to 0.94, while the ratios of $Cl^-/(Cl^-{+}HCO_3^-)$ anion mass concentration ranged from 0.06–0.52 and 0.12–0.99 (Fig. 7). The range of variation is substantial. The distribution of unconfined and confined water samples appears relatively dispersed, with 39.13% of unconfined water samples and 100% of confined water samples exhibiting a $Na^+/(Na^+{+}Ca^{2+})$ ratio greater than 0.6. This may be attributed to cation exchange during the flow of unconfined and confined water or possibly due to human activities. Most unconfined water samples are concentrated in the rock weathering area, indicating that the hydrogeochemical characteristics of unconfined water are primarily influenced by rock weathering (Sui, 2022). Additionally, some unconfined water samples fall within the evaporative concentration area, suggesting that evaporative concentration also contributes to this process. Confined water sampling points are located in areas affected by seawater intrusion and rock weathering, consistent with the distribution characteristics of confined water samples in coastal areas, where aquifers are predominantly brackish and saline water.

In this study, geochemical data were statisti-

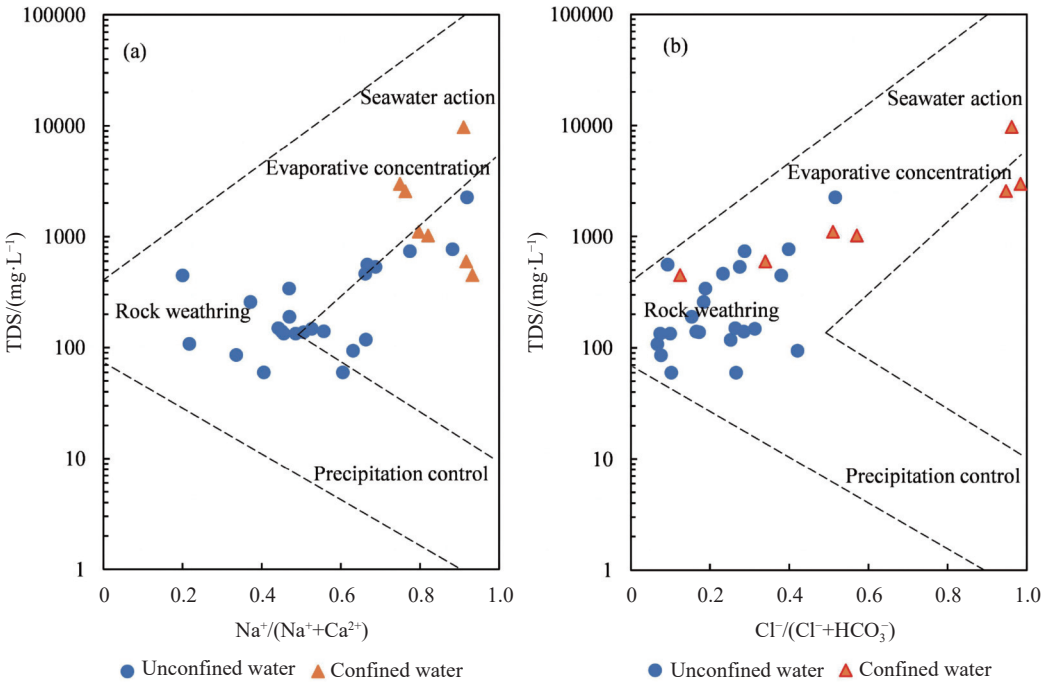


**Fig. 7** Gibbs diagrams of unconfined and confined water

cally processed using Principal Component Analysis (PCA) in IBM SPSS Statistics v.26. PCA is a statistical method that identifies a comprehensive set of variables composed of unrelated original variables based on the interrelationships between the original variables. It condenses the information of the original data, simplifies the structure of the data, and compresses the size of the data (Divya, 2024). PCA can reveal the relationship and control factors among major ionic components in groundwater (Yang et al. 2023). PCA was not conducted for confined water in the study area due to the small number of samples. For the unconfined water samples, 10 variables (TDS, pH, $K^+$, $Na^+$, $Ca^{2+}$, $Mg^{2+}$, $HCO_3^-$, $Cl^-$, $SO_4^{2-}$, $NO_3^-$) from 23 groups were analyzed by principal component analysis. The test results showed that the KMO was 0.594, greater than 0.5, and the Bartlett's test of sphericity showed $p<0.05$, indicating that the research data were suitable for principal component analysis. Three main control factors (PC1, PC2, PC3) were selected based on the principle that the eigenvalue is greater than 1 and the cumulative variance is greater than 80%. The load diagram and Component matrix table are presented in Table 3.

Among the principal component factor PC1 of unconfined water, $K^+$, $Na^+$, $Mg^{2+}$, $Cl^-$, $HCO_3^-$, and TDS show strong positive loads, while $NO_3^-$ shows a moderate negative load. The variance contribution rate of PC1 is 65.26%. This suggests that PC1 may be significantly influenced by the weathering

**Table 3** Table of main ion principal components analysis of groundwater

| Name of index | Loading coefficient | | |
|---|---|---|---|
| | PC1 | PC2 | PC3 |
| $K^+$ | **0.96** | −0.13 | 0.17 |
| $Na^+$ | **0.96** | −0.25 | 0.09 |
| $Ca^{2+}$ | 0.59 | **0.73** | −0.06 |
| $Mg^{2+}$ | **0.98** | −0.12 | 0.10 |
| $Cl^-$ | **0.94** | −0.25 | 0.14 |
| $SO_4^{2-}$ | 0.21 | **0.80** | 0.50 |
| $HCO_3^-$ | **0.97** | 0.01 | −0.06 |
| $NO_3^-$ | −0.53 | −0.25 | 0.53 |
| pH | 0.49 | 0.18 | **−0.68** |
| TDS | **0.99** | −0.11 | 0.12 |
| Characteristic value | 6.53 | 1.45 | 1.07 |
| Variance contribution rate% | 65.26 | 14.47 | 10.74 |
| Accumulating contribution rate% | 65.26 | 79.73 | 90.47 |

of carbonate and halite rocks. During groundwater runoff, water-rock interactions dissolve minerals such as dolomite ($Mg^{2+}$), and Halite ($K^+$, $Na^+$ and $Cl^-$). This indicates that the concentration of $Cl^-$ in groundwater is mainly affected by rock weathering, with the dissolution of dolomite and Halite being the main source of salt in groundwater.

In PC2, $Ca^{2+}$ and $SO_4^{2-}$ show strong positive loads, with a variance contribution rate of 14.47%. Therefore, PC2 also indicates that groundwater salinity is derived from water-rock interaction, and

the dissolution of gypsum is another major factor affecting groundwater salinity.

In PC3, pH shows a moderate negative load wiht the variance contribution rate of 10.74%. This suggests that groundwater pH has a certain effect on groundwater salinity.

### 3.4.2 Water–rock interaction

The milliequivalent ratio, Saturation Index (SI) and cation exchange of main ions in groundwater can provide insights into the influence of water–rock interaction on the origin of main chemical components in groundwater. The chemical composition of groundwater primarily originates from the dissolution of various rock types, including sulfate, halite, carbonate and silicate rocks (Panneerselvam et al. 2020).

(1) Dissolution of halite rocks

The influence of halite or silicate rock dissolution on the source of $Na^+$ in groundwater can be determined based on the ratio of $\gamma(Na^+{+}K^+)/\gamma(Cl^-)$ (Xiao et al. 2015). As depicted in Fig. 8(a), the majority of unconfined water samples in the area are located near the line y=x, indicating that $Na^+$ and $K^+$ ions in unconfined water primarily originate from the dissolution of halite, possibly accompanied by the dissolution of silicate rocks or cation exchange. The Saturation Index (SI) of halite, as shown in Fig. 9(a), indicates that all unconfined water sampling points are in an unsaturated state, confirming that halite is indeed the source of $Na^+$ and $K^+$ in unconfined water.

In contrast, most confined water samples in the study area are distributed below the y=x line, suggesting that the concentration of $Cl^-$ ions in groundwater is significantly higher than the combined concentration of $Na^+$ and $K^+$ ions. In addition, referring to Fig. 9(a), it can be observed that all confined water sampling points tend to be saturated or are already saturated. These findings suggest that, besides the dissolution of halite rocks contributing some ions to the groundwater, the primary source of $Na^+$ and $K^+$ ions is likely external input, such as seawater intrusion.

(2) Dissolution of sulfate rocks and carbonate rocks

The $Ca^{2+}$ and $Mg^{2+}$ ions in groundwater primarily originate from the dissolution of carbonate and sulfate rocks (Wang et al. 2023). Through the analysis of the $\gamma(Ca^{2+}{+}Mg^{2+})/\gamma(HCO_3^-{+}SO_4^{2-})$ ratio depicted in Fig. 8(b), the unconfined water samples are distributed near the y=x line were observed. This suggests that the $Ca^{2+}$ and $Mg^{2+}$ ions in groundwater originate from both the dissolution of carbonate rocks and sulfate rocks. Further analysis of the SI of dolomite, calcite, and gypsum reveals that most of the unconfined water samples are in an unsaturated state for dolomite and calcite. Among these, some samples tend towards precipitation in terms of their dolomite and calcite saturation indices (Fig. 9). However, for gypsum, all unconfined water samples show an unsaturated state, indicating continuous dissolution of gypsum. Therefore, it can be inferred that the important ions in unconfined water primarily originate from the

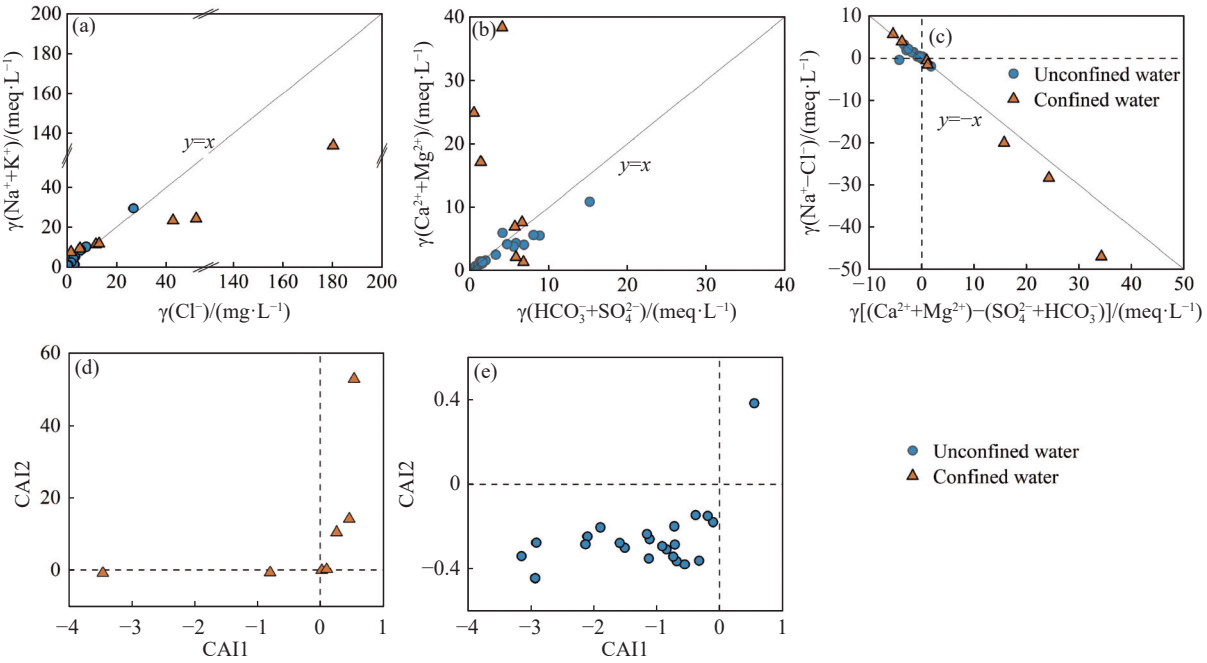


**Fig. 8** The ratio plots of major ion in groundwater and chlor-alkali index diagram

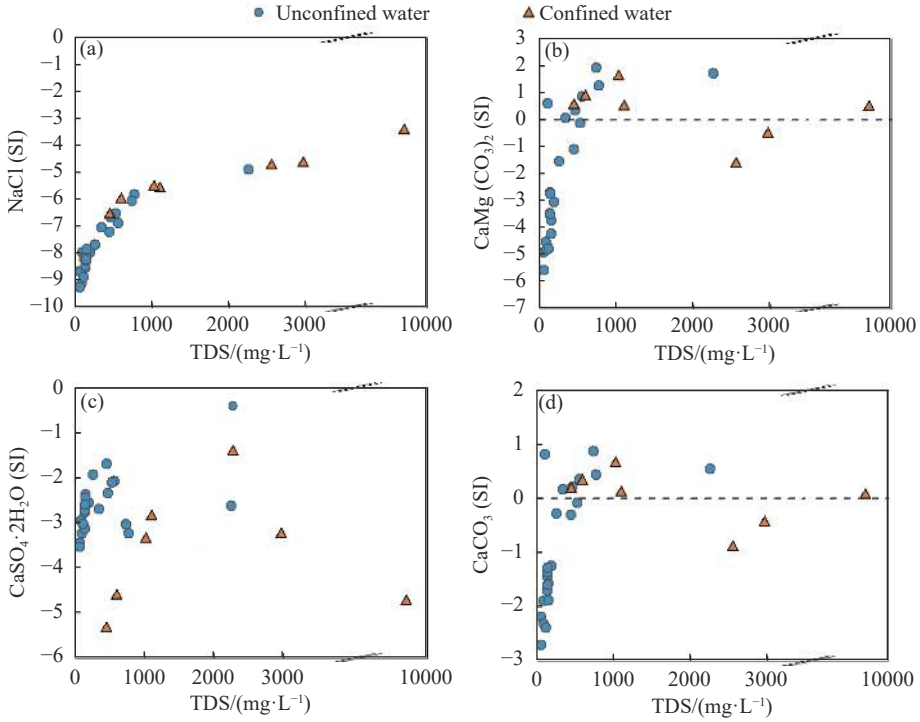


**Fig. 9** The concentration relationship between SI and TDS of main minerals

dissolution of sulfate minerals like gypsum, with a partial contribution from carbonate rocks.

On the other hand, the $\gamma(Ca^{2+}+Mg^{2+})/\gamma(HCO_3^- + SO_4^{2-})$ ratio of confined water samples is mainly located above the y=x line. Simultaneously, with the increase of groundwater depth, most confined water samples tend towards precipitation in terms of their dolomite and calcite saturation indices, while all samples remain in an unsaturated state for gypsum. This phenomenon suggests that the important ions in confined water primarily originate from the dissolution of gypsum rocks.

(3) Cation exchange

A diagram showing the relationship between $\gamma(Na^+–Cl^-)$ and $[\gamma(Ca^{2+}+Mg^{2+})–\gamma(SO_4^{2-}+HCO_3^-)]$ was used to test whether the hydrochemical composition of groundwater was affected by cation exchange (Huang et al. 2020). Cation exchange occurs in aquifers if the ratio between $\gamma(Na^+–Cl^-)$ and $[\gamma(Ca^{2+}+Mg^{2+})–\gamma(SO_4^{2-}+HCO_3^-)]$ is approximately −1 (Zhai et al. 2022). As shown in Fig. 8(c), unconfined and confined water samples are distributed near the cation exchange line (y = –x), indicating that the concentration of $Na^+$ in groundwater decreases with the increase of $Ca^{2+}$ and $Mg^{2+}$, and $Na^+$ in the soil around groundwater is exchanged by $Ca^{2+}$ and $Mg^{2+}$ in the water. The results demonstrate that cation exchange takes place in the unconfined and confined water in study area.

The chloro-alkaline indices can be used to determine the intensity and direction of cation exchange in groundwater. For example, if *CAI1* and *CAI2* are both positive, $Na^+$, $K^+$ in the aquifer media exchanges with $Ca^{2+}$, $Mg^{2+}$ in groundwater, whereas two negative indices indicate the reverse reaction. In addition, higher absolute values of *CAI1* and *CAI2* the chloride index indicate greater degree of ion exchange (Subba Rao et al. 2022).

The chloro-alkaline indices are defined as follows:

$$CAI1 = [Cl^- (Na^+ + K^+)]/Cl^- \quad (2)$$

$$CAI2 = [Cl^- - (Na^+ + K^+)]/\left(SO_4^{2-} + HCO_3^- + CO_3^{2-} + NO_3^-\right) \quad (3)$$

Where: the unit of all ions is meq·$L^{-1}$.

As showed in Fig. 8 (d) and Fig. 8 (e), when comparing unconfined and unconfined water, cation exchange in confined water is more intense. The results indicate that *CAI1* and *CAI2* values are less than zero in 95.65% of unconfined water samples, suggesting that positive cation exchange operates mainly in unconfined water.

The absolute values of *CAI1* and *CAI2* are higher in unconfined water sites near bedrock mountains. indicating that $Ca^{2+}$ exchange $Na^+$ is the strongest in confined water at these locations. *CAI1* and *CAI2* in 28.57% of confined water samples are negative values, suggesting that reverse cation exchange operates mainly in confined water. From the piedmont area to the coastal area, the absolute values of *CAI1* and *CAI2* in confined water gradu-

ally increase, with the highest absolute value located at the river estuary. This result may have been influenced by the effect of seawater intrusion.

#### 3.4.3 Human factors

Studies have indicated that when $NO_3^-$ concentration in groundwater exceeds 5 mg/L, it is considered to be influenced by human activities such as fertilizer application and domestic sewage discharge (Liu, 2020). $SO_4^{2-}$ in groundwater primarily originates from atmospheric deposition, dissolution of sulfur-containing minerals, and industrial activities, etc. The ratio relationship between $SO_4^{2-}/Na^+$ and $NO_3^-/Na^+$ is often used to assess the impact of human activities on groundwater chemistry. A high $SO_4^{2-}/Na^+$ ratio and a low $NO_3^-/Na^+$ ratio suggest a greater influence of industrial activities on groundwater. Conversely, a low $SO_4^{2-}/Na^+$ ratio and a high $NO_3^-/Na^+$ ratio indicate a greater impact from agricultural activities and domestic sewage discharge. When both ratios are higher, it indicates a mixed influence of industrial activities, agricultural activities and domestic discharge on groundwater composition. As depicted in Fig. 10 (a), the two ratios of unconfined water exhibit a positive correlation, suggesting that the chemical evolution of unconfined water in this area may be jointly influenced by industrial activities, agricultural activities and domestic sewage discharge. In contrast, both ratios of confined water are low, indicating that confined water is relatively less affected by human activities.

The main source of $Cl^-$ can be determined by assessing $\gamma(Cl^-)/\gamma(NO_3^-)$. $NO_3^-$ is a typical component of man-made pollution. If $Cl^-$ in groundwater is influenced by human input, $\gamma(Cl^-)/\gamma(NO_3^-)$ would show a positive correlation. As showed in Fig. 10 (b), $\gamma(Cl^-)/\gamma(NO_3^-)$ in both unconfined and confined water does not exhibit an increase with the rise of $\gamma(NO_3^-)$. There is no linear relationship observed between $\gamma(Cl^-)$ and $\gamma(NO_3^-)$, suggesting that the source of $Cl^-$ in groundwater is minimally affected by human activities overall.

#### 3.4.4 Seawater intrusion

Seawater intrusion is a coastal phenomenon triggered by extensive groundwater extraction, leading to a significant decline in groundwater levels and the disruption of the hydrodynamic equilibrium between seawater and freshwater, resulting in the inland movement of the brackish-freshwater boundary (Liu et al. 2017). Confined water primarily occurs in coastal areas and the elevated levels of $Na^+$ and $Cl^-$ indicate potential seawater incursion affecting the confined water.

In freshwater environments, the concentration of $Br^-$ is typically negligible, while seawater exhibits a $Br^-/Cl^-$ ratio around 0.0034. The ratio serves as an indicator to assess whether groundwater salinity is influenced by seawater intrusion (Leybourne, 2008). If $Cl^-$ enrichment in groundwater results from seawater incursion, the $Br^-/Cl^-$ ratio remains consistent despite variations in $Cl^-$ concentration. As illustrated in Fig. 11, the $Br^-/Cl^-$ ratio fluctuates significantly in unconfined points, while most confined water point cluster ground 0.0034, indicating that the $Cl^-$ concentration in confined water is greatly affected by seawater intrusion or remnants of Quaternary transgressions and regressions.

Using the Nemello index method combined with GIS software, five chemical indices, $Cl^-$, TDS, $SO_4^{2-}$, $\gamma Cl^-/\gamma HCO_3^-$, and SAR were selected as evaluation factors. The classification indices for evaluation factors are presented in Table 5. The extent of seawater intrusion was assessed separately for 23 sets of submersible water samples and 7 sets of confined water samples in the study area. As depicted in Fig. 12, seawater intrusion predominantly occurs in the river estuary area of coastal

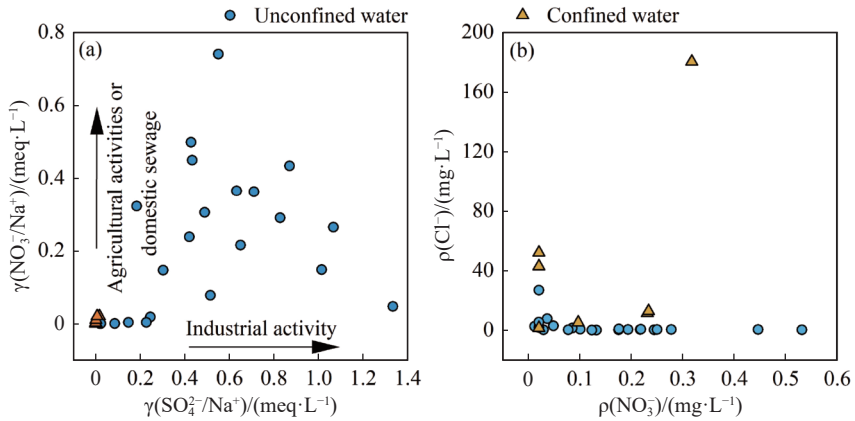


**Fig. 10** The ratio plots of $\gamma(SO_4^{2-}/Na^+)$ and $\gamma(NO_3^-/Na^+)$, $Cl^-$ and $NO_3^-$ in unconfined and confined water

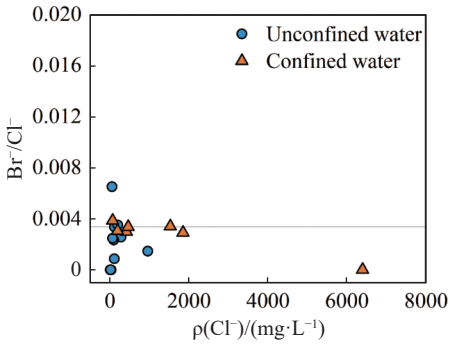


**Fig. 11** The ratio plots of $Br^-/Cl^-$and $Cl^-$ in unconfined and confined water

plain, with confined water being more susceptible to seawater intrusion than unconfined water. Groundwater extraction activities in the Wenzhou area commenced in the 1980s, primarily to meet the domestic water needs of local residents. However, with the rapid economic development of urban and rural areas, there has been a sharp increase in water demand, leading to a notable increase in both the volume of groundwater extraction and the number of extraction wells. According to incomplete statistics, by 2005, the volume of groundwater extraction in this area had reached $2{,}341\times10^4$ $m^3$. Notably, in the Yongqiang Street area of Longwan District, excessive groundwater extraction has led to the formation of a prominent regional groundwater depression cone (Luo, 2015). The center of this cone aligns closely with the intrusion zone identified in the assessment of seawater intrusion in the unconfined aquifer. In this evaluation, modern seawater intrusion of unconfined water mainly occurred in Xiaotang country intrusion section.

During the latter part of the early Late Pleistocene, temperatures gradually warmed, leading to a significant rise in sea levels. The rise extended at least to the vicinity of Xinqiao Town's borehole No. 29, resulting in seawater intrusion. Marine clayey subsoil gradually developed the sand and gravel layer, mixing or intercalating with upstream fluvial deposits to form a fluvial-marine deposit layer. This newly formed layer acts as the aquitard for the confined aquifer in the plain area (Sun, 1980). In this evaluation, the paleoseawater transgression in the late Pleistocene confined aquifer primarily occurred in the Lingkun Island intrusion section, spanning from Qiligang Town to Liusheng Town, and from coastal development zone to Jiya.

## 4 Conclusions

(1) The groundwater samples in study area were observed to be neutral to slightly alkaline. In unconfined water, the predominant cations and anions are $Na^+$ and $HCO_3^-$, respectively. The chemical types of unconfined water are predominantly $HCO_3$-Ca·Na, $HCO_3$·Cl-Na·Ca and $HCO_3$·$SO_4$-Ca·Na. Conversely, in confined water, the dominant cations and anions are $Na^+$ and $Cl^-$, respectively, with chemical types mainly being Cl·$HCO_3$-

**Table 4** Classification and representative value of seawater intrusion index

| Characterization factors (mg·L⁻¹) | No seawater intrusion | Mild seawater intrusion | Moderate seawater intrusion | Severe seawater intrusion |
|---|---|---|---|---|
| $Cl^-$ | ≤250 | ≤600 | ≤1,500 | >1,500 |
| TDS | ≤1,000 | ≤2,000 | ≤3,000 | >3,000 |
| $SO_4^{2-}$ | ≤200 | ≤450 | ≤1,200 | >1,200 |
| $\gamma Cl^-/\gamma HCO_3^-$ | ≤0.5 | ≤1 | ≤6.6 | >6.6 |
| SAR | ≤2 | ≤3.55 | ≤10 | >10 |

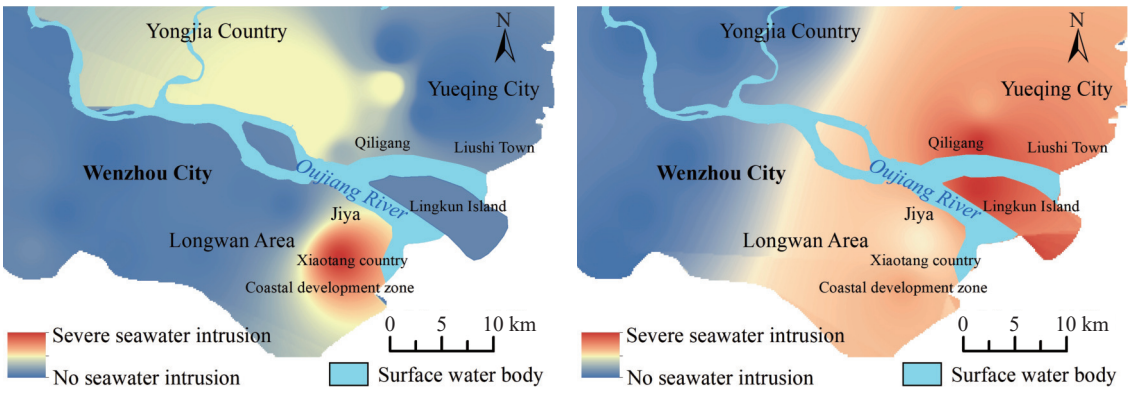


**Fig. 12** Spatial distribution map of seawater intrusion for unconfined (left) and confined water (right)

Na and Cl-Na. Furthermore, there is a gradual shift in the dominant anion in groundwater from $HCO_3^-$ to $Cl^-$ from the mountain front to the coastal area.

(2) Brackish water proportion in unconfined water is relatively low in the study area, whereas confined water exhibits higher salt content, including brackish and saline water. The spatial correlation between TDS, $Na^+$ and $Cl^-$ in groundwater is notably strong. In unconfined water, there is a general trend of higher concentrations in the southeast and lower concentrations in the northwest. As groundwater moves from the mountain to the coastal areas, it tends to become more saline. Additionally, confined water generally exhibits higher ion concentrations compared to unconfined water, displaying interphase distribution characteristics of high and low values.

(3) The salinity of groundwater in the study area is primarily influenced by water-rock interaction involving halite and gypsum, cation exchange, and other factors such as seawater intrusion. Additionally, the salinity of unconfined water is also influenced by the dissolution of carbonate and human activities. Seawater intrusion is identified as the primary factor contributing to the higher salinity of confined water compared to unconfined water. Furthermore, there is a gradual increase in both cation exchange and seawater intrusion gradually from unconfined water to confined water.

(4) Modern seawater intrusion of unconfined water predominantly occurred in the Xiaotang country intrusion section. Halite dissolution and seawater intrusion are identified as the main sources of salt in confined water. Moreover, the paleoseawater transgression in the late Pleistocene confined aquifer primarily occurred in the Lingkun Island intrusion section, spanning from Qiligang Town to Liusheng Town, and from the coastal development zone to Jiya.

## Acknowledgments

This study was supported by investigation project of China Geological Survey (DD20230507).

## References

Alhassan HI, Muntasir AS, Wesam M. 2018. Hydrochemical characterization of groundwater in Balad district, Salah Al-Din Governorate, Iraq. Journal of Groundwater Science and Engineering, 6(4): 306−322 DOI：10.19637/j.cnki.2305-7068.2018.04.006.

Bahir M, Ouhamdouch S. 2020. Groundwater quality in semi-arid environments (Essaouira Basin, Morocco). Carbonates Evaporites, 35: 1−16. DOI：10.1007/s13146-020-00576-7.

Dang XZ. 2022. The formation and evolution mechanism of saline groundwater since Hlocene in Luanhe River Delta, China. Ph. D. thesis. Wuhan: China University of Geosciences Wuhan: 2−3. (in Chinese) DOI：10.27492/d.cnki.gzdzu.2022.000142.

Divya P, Padmaja P, Debjani C. 2024. Groundwater quality evaluation of Narmada district, Gujarat using principal component analysis. Groundwater for Sustainable Development, 24: 101050. DOI：10.1016/j.gsd.2023.101050.

Ez-Zaouy Y, Bouchaou L, Saad A, et al. 2022. Morocco's coastal aquifers: Recent observations, evolution and perspectives towards sustainabilit. Environmental pollution (Barking, Essex: 1987), 293: 118498. DOI：10.1016/j.envpol.2021.118498.

Gang S, Jia T, Deng Y, et al. 2023. Hydrochemical characteristics and formation mechanism of groundwater in Qingdao City, Shandong Province, China. Water, 15 (1348): 1348. DOI: 10.3390/w15071348

Gibbs RJ. 1970. Mechanisms controlling world water chemistry. Science (New York, NY), 170 (3962): 1088−1090. DOI：10.1126/science.170.3962.1088.

Huang WW, Jiang CL, Chen X. 2020. Chemical characteristics and genesis of deep groundwater in the Xinji mining area. Earth and Environment, 48(4): 432−442. DOI：10.14050/j.cnki.1672-9250.2020.48.075.

Jabed MA, Paul A, Nath TK. 2018. Peoples' perception of the water salinity impacts on human health: A case study in south-eastern coastal region of Bangladesh. Exposure and Health, 12(1): 41−50. DOI：10.1007/s12403-018-0283-0.

Jia HY, Chu M. 2007. Present situation and countermeasures of groundwater exploitation and utilization in Wenzhou city. Zhejiang Hydrotechnics, 2007, 35(5): 65−69 (in Chinese) DOI：10.13641/j.cnki.33-1162/tv.2007.05.028.

Kazakis N, Pavlou A, Vargemezis G, et al. 2016. Seawater intrusion mapping using electrical resistivity tomography and hydrochemical

data. An application in the coastal area of eastern Thermaikos Gulf, Greece. Science of the Total Environment, 543: 373−387. DOI：10.1016/j.scitotenv.2015.11.041.

Larsen F, Tran LV, Van H, et al. 2017. Groundwater salinity influenced by Holocene seawater trapped in incised valleys in the Red River delta Plain. Nature Geoscience, 10: 376−381. DOI：10.1038/NGEO2938.

Leybourne M, Goodfellow WD, View C. 2008. Br/Cl ratios and O, H, C, and B isotopic constraints on the origin of saline waters from eastern Canada. Geochimica et Cosmochimica Acta, 71(9): 2209−2223. DOI：10.1016/j.gca.2007.02.011.

Li W, Liu J. 2023. Contamination, sources and leval of heavy metals in the sediments of Oujiang River. Journal of Xinyang Normal University, 36(2): 274−279. (in Chinese) DOI：10.3969/J.issn.1003-0972.2023.02.019.

Liu JT. 2020. Hydrochemical evolution mechanism and optimization of monitoring network for groundwater in Pearl River Delta, China. Ph. D. thesis. Xi'an: Northwest University: 100. (in Chinese) DOI：10.27405/d.cnki.gxbdu.2020.002275.

Liu Y, Jiao JJ, Liang W, et al. 2017. Hydrogeochemical characteristics in coastal groundwater mixing zone. Applied Geochemistry, 85 (Part A): 49−60. DOI：10.1016/j.apgeochem.2017.09.002.

Lou MF. 2015. The preliminary study of land subsidence in Yongqiang plain Wenzhou city Zhejiang Province. The Chinese Journal of Geological Hazard and Control, 26(3): 133−139. (in Chinese) DOI：10.16031/j.cnki.issn.1003-8035.2015.03.24.

Pan LS. 2020. Evaluation of groundwater quality. Metallurgical management, (1): 154, 24. (in Chinese)

Panneerselvam B, Paramasivam SK, Karuppannan S, et al. 2020. A GIS-based evaluation of hydrochemical characterisation of groundwater in hard rock region, South Tamil Nadu, India. Arabian Journal of Geosciences, 13 (17): 1−22. DOI: 10.1007/s12517-020-05813-w

Sheng D, Meng X, Wen X, et al. 2023. Hydrochemical characteristics, quality and health risk assessment of nitrate enriched coastal groundwater in northern China. Journal of Cleaner Production, 403: 136872. DOI：10.1016/j.jclepro.2023.136872.

Subba Rao N, Dinakar A, Sun L. 2022. Estimation of groundwater pollution levels and specific ionic sources in the groundwater, using a comprehensive approach of geochemical ratios, pollution index of groundwater, unmix model and land use/land cover – A case study. Journal of Contaminant Hydrology, 248: 103990. DOI：10.1016/j.jconhyd.2022.10399.

Sui Y. 2022. Hydrochemical characteristics and genetic analysis of karst water in Tai'an City, Shandong Province. International Core Journal of Engineering, 8(4): 816−828. DOI：10.6919/icje.202204_8(4).0097.

Sun L. 1980. A regional hydrogeological survey report of 1: 200,000 scale for H-51-31 Wenzhou and H-51-32 Huangyan maps in Zhejiang Province. Zhejiang Institute of Hydrogeology and Engineering Geology, 47. (in Chinese)

Sun Q, Gao M, Wen Z, et al. 2023. Hydrochemical evolution processes of multiple-water quality interfaces (fresh/saline water, saline water/brine) on muddy coast under pumping conditions. Science of the Total Environment, 857: 159297. DOI：10.1016/j.scitotenv.2022.159297.

Thilagavathi R, Chidambaram S, Ganesh N, et al. 2021. Geochemical variations due to salinization in groundwater along the southeast coast of India. SN Applied Sciences. 3(5): 1−15. DOI:10.1007/s42452-021-04551-2

Trabelsi R, Zouari K. 2019. Coupled geochemical modeling and multivariate statistical analysis approach for the assessment of groundwater quality in irrigated areas: A study from North Eastern of Tunisia. Groundwater for Sustainable Development, 8: 413−427 DOI：10.1016/j.gsd.2019.01.00.

Troudi N, Hamzaoui-Azaza F, Tzoraki O, et al. 2020. Assessment of groundwater quality for drinking purpose with special emphasis on salinity and nitrate contamination in the shallow aquifer of Guenniche (Northern Tunisia). Environmental monitoring and assessment, 192 (10): 641. DOI：10.1007/s10661-020-08584-9.

Wang S, Chen J, Zhang SX, et al. 2023. Hydrochemical evolution characteristics, controlling factors, and high nitrate hazards of shallow groundwater in a typical agricultural area of Nansi Lake Basin, North China. Environmental Research. 223: 115430. DOI：10.1016/j.envres.2023.115430.

Wang XY. 2019. Hydrochemical characteristics of groundwater in Heihe River Basin, Shaanxi, China. Journal of Desert Research, 39(4): 168−176. DOI：10.7522/j.issn.1000-694X.2019.00028.

Xiao J, Jin Z. D, Wang J, et al. 2015. Hydrochemical characteristics, controlling factors and solute sources of groundwater within the Tarim River Basin in the extreme arid region, NW Tibetan Plateau. Quaternary International, 380-381: 237−246. DOI：10.1016/j.quaint.2015.01.021.

Yang Z, Hu L, Ma H, et al. 2023. Hydrochemical characteristics of groundwater and their significance in arid inland hydrology. Water, 15 (1641): 1641. DOI：10.3390/w15091641.

Zamrsky D, Karssenberg ME, Cohen KM, et al. 2020. Geological heterogeneity of coastal unconsolidated groundwater systems worldwide and its influence on offshore fresh groundwater occurrence. Frontiers Earth Science, 7: 1−23. DOI：10.3389/feart.2019.00339.

Zhai Z, Zhang C, Tang T, et al. 2022. Hydrochemical characteristics and genetic analysis of shallow high-fluorine groundwater in Fuyang River Basin. Geofluids, 2022: 9682371. DOI：10.1155/2022/9682371.

Zhang B, Song XF, Han DM, et al. 2013. Seawater intrusion degree evaluation based on mathematical statistics and fuzzy mathematics in Qinhuangdao Yangdai River Plain. Scientia Geographica Sinca, 33(3): 342−348. DOI：10.13249/j.cnki.sgs.2013.03.001.

Zhang Y, Fu CC, Mao L, et al. 2017. Hydrochemical characteristics and formation mechanism of the grounwater in YanChe, Jiangsu Province. Resources and Environment in the Yangtze Basin, 26(4): 598−605. DOI：10.11870/cjlyzyyhj201704013.

Zhu XX. 2009. Environmental geological survey and evaluation report of Wenzhou City, Zhejiang Province. Zhejiang provincial geological environment monitoring station, 30−31. (in Chinese)